Tuning of the chiral nematic phase of cellulose nanocrystals by the adsorption of a short polymer on their surface

Hugo Voisin, Adèle Vasse, Estelle Bonnin, Fabrice Cousin, Isabelle Capron

Tuning of the chiral nematic phase of cellulose nanocrystals by the adsorption of a short polymer on their surface

Hugo Voisin
INRAE, UR BIA
Adèle Vasse
INRAE, UR BIA
Estelle Bonnin
INRAE, UR BIA
Fabrice Cousin
CEA Saclay
Isabelle Capron (isabelle.capron@inrae.fr)
INRAE, UR BIA

Research Article

Keywords: self-assembly, nanoparticle, chiral nematic phase, cholesteric pitch, chiral strength, small angle x-ray scattering

Posted Date: May 19th, 2023

DOI: https://doi.org/10.21203/rs.3.rs-2938491/v1

Abstract

Concentrated cellulose nanocrystals (CNC) suspensions are known to self-assemble into liquid crystalline cholesteric phase. However, the origin of this chirality transfer is still matter of discussion. In this work, we used a tailor-made biopolymer, xyloglucan (XG), at a very small molar mass (20,000 g/mol) that adsorb flat on the cellulose surface. We showed that the addition to a dispersion of CNC at 60 g/L of XG up to 10 g/L decreased the anisotropic volume fraction, increased the cholesteric pitch, and kept constant the inter-CNC distance implying a change in the twist angle and a lower chiral strength. These results indicate that a very limited modification of CNC in surface can induce important variation of the cholesteric order. Above 10 g/L XG, XG-covered CNCs decreased the cholesteric pitch and preferentially concentrated in the isotropic phase, decreasing the global cholesteric liquid crystal (CLC) order.

Introduction

Nature is full of highly anisotropic and oriented materials that present peerless optical and mechanical properties. Several biologic systems are hierarchically structured (Jiang et al. 2020).Notably, the chiral self-assembly of nanoscale building blocks is a universal phenomenon that allows large-scale structures with properties that are issued from the individual subunits (Mitov 2017).

Cellulose nanocrystals (CNC) obtained from hydrolysis of wood fibers, are nanorods of approx. 6 nm wide for 100–200 nm in length with a facetted crystalline structure. Obtained through sulfuric acidic hydrolysis, CNCs are negatively charged due to sulfate half-ester groups on their surface, making it possible to obtain stable colloidal suspensions in water. At higher concentration (above 3 to 8 wt. % according to the source), CNC spontaneously separate in two phases following a first-order transition (Honorato-Rios et al. 2016), with a less concentrated isotropic phase upward, and an anisotropic phase that sediments and forms a homogeneous anisotropic phase at the bottom of a container. In the anisotropic phase, they spontaneously self-assemble to form left-handed chiral nematic (cholesteric) phase, with a long-range orientational order, *i.e.* they tend to align themselves along a common direction (Dong et al. 1996). This direction, represented by the director vector, rotates along a vector called the cholesteric axis, forming the so-called cholesteric phase. The strength of the chiral interactions in CNC suspensions can be assessed by measuring both the chiral nematic pitch (corresponding to the period of one full rotation of the helicoidal structure), typically in the range of 5–50 µm, and the interparticle distance, in the range of 25 to 50 nm. A change of pitch at a given CNC concentration implies a variation of twisting angle between CNC (Schütz et al. 2015), related to the strength of the chiral interaction.

First described by Revol et al. (Revol et al. 1992), the origin of the chirality of this cholesteric phase, or more accurately the transfer mechanism of the intrinsic chirality of the cellulose molecule to the supramolecular assembly of the CNCs, is still subject to debate. It has been theorized that the chirality was transferred between adjacent CNC through electrostatic repulsion (Orts et al. 1998) (Araki and Kuga 2001); however, the observation of cholesteric phase of hydrophobically functionalized CNCs in toluene, an apolar solvent, refuted this explanation (Heux et al. 2000; Elazzouzi-Hafraoui et al. 2009).

From the literature, a correlation between mean particle length and helicoidal twisting power with longer particles accumulated in the anisotropic phase was established (Honorato-Rios et al. 2018). More recently, Parton et al. studied shape variation of CNCs by comparing a liquid crystalline (LC) phase obtained from individual crystallite particles and bundles that are stair-like association of CNCs with larger aspect ratios. Bundles were preferentially partitioned in the anisotropic phase, highlighting morphological specificities as responsible for chirality (Parton et al. 2022).

While ionic strength is known to strongly impact the liquid crystalline state of CNCs (Dong et al. 1996), neutral hydrosoluble polymers have also displayed an influence. Two cases might be considered: interacting or non-interacting polymers. In the first case, the polymer might be adsorbed through enthalpically attractive or entropically favorable interactions, and will generate either steric repulsion or inter-CNC bridging mechanisms according to the polymer chain length versus the CNC/polymer ratio (Dammak et al. 2015) which might lead to large aggregation. Formation of a uniform coating of polydopamine has shown to preserve the cholesteric organization, with an increased pitch (Dong et al. 2020). The polymer functionalization could also be obtained through covalent grafting, such as PEO grafting which caused a reduction of the cholesteric pitch. In the case of non-interacting polymers, the phase separation generally observed is explained through depletion force caused by the free polymer that leads to CNC aggregation (Sun et al. 2022). The aforementioned mechanisms involved the influence of CNC morphology, salt, and added polymers on CNC CLC behavior. However, no work has described the change in chemical surfaces of the CNC by self-assembly of polymers laying flat onto the CNC surface, *i.e.* where the adsorbed chains are mostly in train than in loops.

We recently studied the assemblies of xyloglucan (XG) a hemicellulose whose interaction with cellulose surface is generally considered irreversible and entropically driven, with CNC. We showed that short xyloglucan (XG) chains, with molar masses of 20,000 g/mol, which corresponds to an average backbone length of 33 nm or 66 glucoses, had limited impact on the colloidal LC state of concentrated (70 g/L) suspension of CNCs on a wide range of XG concentration, leaving their viscosity unchanged and free to relax into CLC. On the opposite, chains of 30,000 g/mol and 40,000 g/mol (average backbone length of 66 nm or 132 glucoses) disrupted the LC organization up to a glassy or gel arrested state, respectively, even at low XG concentration (Voisin et al. 2023). We demonstrated that short XG mainly adsorbed as trains on CNC surface, whereas longer XG formed tail conformation. This very low Mw corresponded to a narrow window of molar mass above the minimal M_w required for XG adsorption (Lopez et al. 2010) and below the formation of tail conformation.

In this article, very short XG (15,000–20,000 g/mol) were adsorbed onto CNC surface, modifying the chemical surface of CNCs without increasing their hydrodynamic radius as confirmed by absence of enzymatic degradation of CNC-XG in presence of endoglucanase, no change in rheological moduli, DLS measurements and STEM dimensions. Anisotropic CNC suspensions were prepared with XG added in a range of concentration from 1 to 30 g/L. The XG-decorated CNCs were dispersed at sufficiently high concentration (60 g/L) to reach CLC organization. This study, comparing the anisotropic volume fraction, the pitch and the inter-CNC distance reveals that a slight modification of the surface of the CNC,

adsorbing a short chain of XG, decrease the volume fraction of anisotropic phase, increase the pitch of CLC organization but preserve constant the inter-CNC distance. With this set-up, these results aim to provide new insights in the understanding of the chirality transfer in the anisotropic cholesteric phase.

Materials and Methods

Materials.

Wood sulfated CNC in sodium form were purchased from Celluforce (Montreal, QC, Canada). They presented typical length of 165 ± 82 nm, cross section of 6 ± 2 nm (estimated from STEM observation over 100 particles) and sulfur content of approx. 0.6 wt % (obtained from elementary analysis). They have an estimated sulfur content of 0.25 mmol/g, meaning that a 60 g/L CNC suspension presents an ionic strength in the 15-17.5 mM range. They were used as received without dialysis. Native XG from tamarin seed (Mw ≈ 850 000 g/mol) was purchased from DSP Gokyo Food & Chemical Co., Ltd. Osaka, Japan.

Preparation of CNC and XG.

Preparation of short XG. Low M_w XG were prepared by enzymatic degradation of native XG to reach 20,000 g/mol (XG_{20}). Solutions at 10 g/L native XG were prepared by dissolving the powder in milli-Q water under magnetic stirring at 50°C for 2 hours, then at room temperature overnight. Typical volume for enzymatic degradation was 10 mL. The required volume of *Trichoderma longibrachiatum* solution was then added to the XG solution, to obtain 1 unit of CELTR per gram of XG. The reaction medium was incubated at 40°C on a stirring wheel at 20 rpm for 4 hours. It was then heated at 100°C for 10 minutes to inactivate the enzyme. The low M_w XG were then purified by precipitation in 4°C ethanol (ratio water:ethanol is 40:60) by stirring the mixture for 10 minutes and resting overnight. It was then centrifugated at 17,500 g for 30 minutes. The precipitate was redispersed in water and the ethanol was evaporated using rotary evaporator. The M_w distribution was measured using HPSEC-RALS. The resulting solutions were then frozen and freeze-dried.

Preparation of CNC suspensions and CNC-XG mixtures. CNC suspensions were prepared at the desired concentration by dispersing adequate CNC mass into milli-Q water, free from added salt, using magnetic stirring followed by ultrasonication using Q700 sonicator (20 kHz, 700 W maximum output, Qsonica LLC, Newtown, CT). The dispersion was performed using a power of at least 40 W and 2 kJ/g CNC. XG solutions were prepared at the desired concentration by dissolving the freeze-dried powder at 1.41 g/L. CNC suspension and XG solution were mixed using a vortex mixer then sonicated (power ≈ 10 W, energy ≈ 200 J/mL suspension) and briefly centrifuged on a benchtop centrifuge to remove air bubbles.

Characterization Methods.

High-Performance Size-Exclusion Chromatography (HPSEC). XG samples were dissolved at 5 g/L in 50 mM $NaNO_3$ (99% Sigma Ultra S8170-250G) and filtered at 0.45 µm on PVDF membrane before analysis.

The eluent consisted of 50 mM $NaNO_3$ and was filtrated through a 0.1 µm pore membrane. The samples were eluted at 0.7 mL/min on a Shodex OHpak SB-805 HQ column (8 mm × 300 mm). The online molar mass, refractive index, and intrinsic viscosity were measured on a multidetector system OMNISEC Malvern consisting of a right-angle laser light scattering (RALS) detector, a differential refractometer, and a differential viscometer. Molar masses were determined by using ASTRA 1.4 software (Wyatt, USA). The concentrations of eluted XG were calculated by using a refractive index increment dn/dc = 0.147 mL/g. This method allows an accurate determination of peak concentrations and thus an absolute distribution of molar mass.

SAXS measurements. SAXS measurements were carried out on a Xeuss 2.0 instrument from Xenocs, which uses a microfocused Cu Kα source with a wavelength of 1.54 Å and a PILATUS3 detector (Dectris, Switzerland). The experiments were performed at a sample-to-detector distance of 2487 mm with a collimated beam size of 0.5 × 0.5 mm to achieve a q-range of 0.0045 $Å^{-1}$ – 0.2 $Å^{-1}$. The solutions were poured inside 1.5 mm glass capillaries, filled with at least 10 mm high samples before being sealed using molten paraffin and left to equilibrate 5 days.

Enzymatic degradation of CNC-XG mixtures. CNC (22.5 or 55 g/L final concentration) and XG20 or XG40 (30 g/L final concentration) were mixed as previously described. The suspensions were submitted to enzymatic degradation with GH7 endoglucanase from *Trichoderma longibrachiatum* (E-CELTR, Megazyme) at 0.2 mg/mL final concentration for 4 hours at 40°C. Aliquots were withdrawn at intervals and analyzed for the appearance of reducing ends using Nelson method (Nelson, 1944) after relevant dilution. The absence of activity of the enzyme on CNC was verified beforehand (data not shown). A XG solution at 30 mg/mL was treated in the same conditions as a control experiment. Analyses were performed in duplicates.

Microscopic Observation. To measure the pitch, 80 µL of the suspension were placed on a microscope slide in a 65 µL spacer closed with a 20 x 20 mm microscope cover slip, corresponding to a sample thickness around 300 µm. The samples were kept in an atmosphere saturated in humidity to prevent water evaporation. Comparison with systems in hermetically sealed tubes were performed to assess an eventual loss of water through the spacer, but no differences with the suspensions on glass slides were observed (data not shown). The liquid crystalline organization was estimated after various times of rest, using an upright Olympus system microscope (Model BX51) equipped with a x10 objective and cross polarizers.

Results and Discussion

Microstructure of the CNC-XG assemblies. The short chain XG showed a Mw around 20,000 g/mol and a polydispersity index of 1.34 (Fig. S1). Several batches were used for the study, all validated by this technic. When mixed with CNCs, they systematically led to the same cholesteric results as long as the average M_w was kept above 15,000 g/mol and below 22,000 g/mol. The XG-decorated CNCs hydrodynamic radius were measured through DLS and showed no modification due to XG adsorption as

curves superimposed (Fig. S2). Rheological measurements also revealed the same profiles for pure CNC suspension and CNC-XG mixtures at various XG concentrations (Fig. S3). In order to assess more accurately the conformation of XG on the CNC surface, we performed enzymatic accessibility experiments. Indeed, it was previously shown using longer native XG (Mw = 850 000 g/mol) that, when chains adsorbed as a train on CNC, they could not be hydrolyzed by glucanase, whereas free chains existing as loop or tail were easily degraded (Dammak et al. 2015). We thus exposed two solutions of XG at 20,000 g/mol (XG_{20}) and 40,000 g/mol (XG_{40}) and concentrated at 30 g/L with an increasing concentration of CNCs to a glucanase solution. We confirmed the complete adsorption of XG_{20} in a train conformation at a XG:CNC ratio of 0.55 since no free glucose was detected after hydrolysis even after 240 min of hydrolysis. As a comparison, the same analysis was carried out in the same concentration conditions with a slightly longer XG_{40}. The enzymatic susceptibility demonstrated the existence of a fraction of XG accessible to the enzyme, corresponding to tails or bridging conformations of the XG_{40}, absent with the shorter ones. This is in line with some previous rheological tests that showed a clear gel behavior for XG_{40} (Voisin et al. 2023). These tests thus validated that XG_{20} was fully adsorbed along the CNC.

Influence of XG addition on the liquid crystalline organization of a biphasic CNC suspension. We studied the influence of the addition of XG from 0 to 30 g/L in a suspension of CNC on the phase separation behavior of the CNC and on the features of the cholesteric phase. As usually observed at 60 g/L, pure CNC spontaneously separate in two phases with an anisotropic phase at the bottom of the tube. The lower phase is more birefringent than the isotropic upper phase, can be more clearly differentiated between crossed polarizers (Fig. 2), and the interface visible as a gray meniscus. The volume fraction of anisotropic phase is known to vary with both the CNC concentration until the whole suspension becomes anisotropic, and with the effective aspect ratio that considers the CNCs intrinsic dimension and the electrostatic repulsion applying on a distance scaling with the Debye length of *ca.* 3 nm at 40 g/L CNC and 2.1 nm at 80 g/L CNC, considering the counterions concentration. The addition of XG induced strong variations on the isotropic to anisotropic phase ratio. This was followed by measuring the relative heights of both phases in tubes after 5 days of equilibrium (Fig. 2). Increasing the concentration of XG modified the phase ratio to maximize positional entropy in a progressive way. It was visible that progressive addition of XG in CNC suspension at fixed CNC concentrations led to a decrease of the anisotropic phase fraction from 65 vol% in a XG-free suspension to 33 vol% for both 20 g/L and 30 g/L of XG.

The homogenized suspensions, *i.e.* before equilibration, were observed between glass slides using polarized optical microscopy (Fig. 3). After 4 days of equilibration, isotropic domains appearing as dark and anisotropic cholesteric phase appearing as bright with a characteristic “fingerprint” structure were observed. In the CLC, the distance between two bright lines corresponded to a half cholesteric pitch. For all the studied XG concentration, an anisotropic phase with fingerprints were visible. But increasing XG concentration led to a decrease of the anisotropic volume fraction as well as a disruption of the anisotropic phase into smaller bright domains. This was in good agreement with the results from tubes left at rest 5 days (Fig. 2). Phase separated-droplets were also increasingly observed, visible as dark

circles over the bright anisotropic regions. They were attributed to dispersed fractions of isotropic phase locked into anisotropic phase.

The pitch was determined from image analysis and shown in Fig. 4. After 5 days of equilibration, the addition of XG from 0 to 10 g/L increased the pitch from 12 to 24 µm without variation of hydrodynamic radius (Fig. S2) nor viscosity (Fig. S3). This reflected the progressive covering of the CNC surface by XG, showing that the change of surface chemistry or topology had a strong impact on inter-CNC chiral interactions. At higher XG concentration (above 10 g/L), the pitch decreased back close to its nominal value of 12 µm at 30 g/L. It reflected a change of regime of the XG adsorption; however, enzymatic accessibility experiments (Fig. 1) revealed that no XG was accessible, *i.e.* neither free nor in tail conformation. This pitch decrease was still observed after 11 days of equilibration due to the coalescence and slow global organization of the anisotropic phase.

While our previous study did not indicate any XG-mediated aggregation or precipitation, both the increase of pitch and the decrease of anisotropic phase fraction could be explained by a concentration decrease through decantation. SAXS measurements were performed on capillaries of the CNC-XG suspension stabilized for 4 days in order to obtain information on the suspension microstructure and interparticular distance. Figure 5 displays the Kratky representation of the SAXS data, *i.e.* I(q) x q² as a function of *q*. This representation highlighted the characteristic peaks of the inter-CNC distances, as the form factor of the CNC shows a characteristic q^{-2} decay in this q-range (Haouache et al. 2022). It shows a strong correlation peak at q_0, followed by its harmonics at 2 q_0. The interparticular distance *d* between CNCs was obtained using $d = 2\pi/q_0$. The evolution of *d* as a function of [CNC] and [XG] is plotted in the insets of Fig. 5.

It can be observed that *d* was strongly affected by the CNC concentration, shifting from 29 nm at 40 g/L CNC to 22.8 nm at 80 g/L, which is consistent with previous studies (Schütz et al. 2020). For the XG containing suspensions, XG addition had almost no influence on the interparticular distance that remained nearly constant from 0 to 30 g/L of XG at 26 ± 1 nm. It results that XG only influenced the pitch at constant inter-CNC distance, and implied that XG was affecting the twisting angle between CNC planes along the cholesteric axis. At very high XG concentration, above 10 g/L, the peaks pitch values were decreasing at unchanged *d* value. However, the peaks in SAXS became wider and less defined, indicating either a lower organization or a decrease of the size of the cholesteric domain. This was in good agreement with the heavily distorted anisotropic phase observed in POM (Fig. 3).

We aimed to quantify a possible partition of XG visualizing the mixture of CNC at 60 g/l and FITC-functionalized XG at 10 g/L by fluorescence microscopy. It revealed a clear correlation between the LC organization and the XG concentration. Indeed, it is visible on Fig. 6 that the fluorescence intensity of XG was higher in the isotropic area (darker areas on birefringent image Fig. 6.b) than in the organized areas (brighter areas on Fig. 6.b). It thus demonstrated a non-equal partition of XG as it concentrated in the isotropic phase.

Since we determined on Fig. 1 that all XG chains were adsorbed aligned on the CNCs, the difference of XG concentration did not arise from an accumulation of free XG in the isotropic phase. The increase of XG concentration until 10 g/L corresponded to a regime of progressive covering of CNC surface with XG. Therefore, CNC that did not carry any XG adsorbed chains or not fully saturated coexisted with covered CNCs. It can thus be concluded that the XG-covered CNCs were preferentially concentrated in the isotropic phase. The higher fluorescence intensity was still observed at higher XG concentration (30 g/L) (Fig. S4.a), and the dark droplets visible on Fig. 3 displayed higher fluorescence intensity (Fig. S4.b). This indicated that the XG at the CNCs surface above 10 g/L did not affect all CNCs simultaneously, and that CNCs with higher XG surface density partitioned into the isotropic phase. These results hinted for a phase separation where the XG, even if with very low Mw and well adsorbed, decreased the chirality of the rod, increasing the isotropic fraction.

Hypothesis regarding the XG impact. To summarize the observation, two main domains might be distinguished according to the XG concentration added to CNC: the low concentration (between 0 and 10 g/L) and the higher concentration (above 10 g/l).

At low concentration (between 0 and 10 g/L), the following parameters were observed:

- Decrease of the anisotropic phase fraction
- Increase of the pitch
- Interparticular distance remained unchanged
- XG covered CNCs preferentially partitioned to the isotropic phase

The most intuitive influence of the decrease of the anisotropic phase fraction with adsorption of XG (Fig. 1) would be a decrease of their aspect ratio due to the increase of their effective width. It has indeed been described that the thicker rods concentrated in the isotropic phase (Honorato-Rios et al. 2018). However, it has been described that decreasing the aspect ratio of CNC, usually through their shortening, actually decreased the cholesteric pitch (Beck-Candanedo et al. 2005). Furthermore, we consider that the effective increase of thickness caused by the adsorption of a single XG chain lying flat on cellulose surface would be negligible in regards to the observed effect.

The increase of the cholesteric pitch at equal interparticular distance implies a decrease of the chiral strength ψ, which linearly correlates the volume fraction of a suspension to its chiral nematic wave vector, *i.e.* the chiral interactions between particles were weaker (Harris et al. 1999). This was in line with the hypothesis of the nematic phase induced by spiral like bundles (Parton et al. 2022): adsorption of XG would modify these bundle's chirality either by decreasing their number of by affecting their chiral strength. A decrease of their number might be due to sonication after XG addition and mixing, with a dissociation of the bundle favored by the XG adsorbed on the CNC facets, in a similar fashion to the exfoliation of layered silicate following polymer intercalation (Alexandre and Dubois 2000). We verified this assumption by comparing the aspect of a 60 g/L CNC suspension with 10 g/L XG, but without

sonication after CNC - XG mixing (Fig. S5). No pitch difference was observed when comparing to the sonicated systems, and the reason of the pitch increase must lay elsewhere.

While no definitive proof could be obtained from our results, it appeared that the adsorption of the XG on the bundles surface at low concentration decreased their chirality. This can be induced either by flattening their asymmetrical appearance, by blurring the "twisted raft" shape of the bundle (morphological variation), or by modifying the interaction between the CNCs by screening specific surfaces (chemical variation). However, it is remarkable that this very limited modification induced such important changes in CLC.

At higher XG concentration (above 10 g/L), the pitch decreased and we observed a disruption of the anisotropic phase into smaller bright domains by microscopy. This was difficult to interpret. One hypothesis is that the over-adsorption of XG led to the exposition of some XG side groups, too small to be accessible to enzymes, or to influence the rheological properties and hydrodynamic radius, but increasing sterically the chiral interaction. This would be in line with what had been observed with the chemical grafting of polymers on CNCs which decreased the cholesteric pitch (Azzam et al. 2016). These polymers formed a corona around the CNC in a mushroom conformation, with a radius of gyration of 1.3 nm (Azzam et al. 2020), close to what can be estimated of the 1 to 2 sugars-long XG side groups. It was suggested that the chirality was accentuated due to the steric interactions, and a similar increase of chiral strength could be observed in our system following the increase of the CNC surface roughness.

Conclusion

Using tailor-made polymers in the very low range of molar masses compatible with full adsorption on the CNC surface, we prepared a model system for the study of its influence on CNC cholesteric organization. It appeared that covering CNCs at 60 g/L with a small fraction of XG adsorbed flat decreased the anisotropic volume fraction, strongly increased the cholesteric pitch of the CNCs while retaining the same interparticular distance, implying that it strongly decreased their chiral strength. It revealed that their chiral strength is highly sensitive to slight modification of the CNC surface chemistry such as adsorption of a short polymer chain. On the contrary, adding more XG (above 10 g/L) increased their chiral strength, which then probably involved steric interactions. The explanation of the influence of short XG on the CNCs liquid crystalline behavior would require more investigation through a combination of molecular simulation and experimental methods able to discriminate molecules like small-angle neutron scattering.

Declarations

Acknowledgement

The authors thank Luc Saulnier (BIA-Nantes) for average Mw measurements using SEC-RALS-LALS.

Funding

This work was supported by the Agence Nationale de la Recherche (project Clicteam N° ANR-18-CE09-0028).

Dedication

The authors are grateful to editors to give them the opportunity to contribute to this special issue dedicated to Henri Chanzy since they recognize his huge contribution to carbohydrates science in general and acknowledge him for the numerous scientists that he inspired. We hope that this work will contribute to the continuation of this great story bridging the structure and properties of polysaccharides.

Ethics approval and consent to participate

Not applicable

References

1. Alexandre M, Dubois P (2000) Polymer-layered silicate nanocomposites: Preparation, properties and uses of a new class of materials. Mater Sci Eng R Reports 28:1–63. https://doi.org/10.1016/S0927-796X(00)00012-7
2. Araki J, Kuga S (2001) Effect of trace electrolyte on liquid crystal type of cellulose microcrystals. Langmuir 17:4493–4496. https://doi.org/10.1021/la0102455
3. Azzam F, Frka-Petesic B, Semeraro EF, et al (2020) Small-Angle Neutron Scattering Reveals the Structural Details of Thermosensitive Polymer-Grafted Cellulose Nanocrystal Suspensions. Langmuir 36:8511–8519. https://doi.org/10.1021/acs.langmuir.0c01103
4. Azzam F, Heux L, Jean B (2016) Adjustment of the Chiral Nematic Phase Properties of Cellulose Nanocrystals by Polymer Grafting. Langmuir 32:4305–4312. https://doi.org/10.1021/acs.langmuir.6b00690
5. Beck-Candanedo S, Roman M, Gray DG (2005) Effect of reaction conditions on the properties and behavior of wood cellulose nanocrystal suspensions. Biomacromolecules 6:1048–1054. https://doi.org/10.1021/bm049300p
6. Dammak A, Quémener B, Bonnin E, et al (2015) Exploring architecture of xyloglucan cellulose nanocrystal complexes through enzyme susceptibility at different adsorption regimes. Biomacromolecules 16:589–596. https://doi.org/10.1021/bm5016317
7. Dong XM, Kimura T, Revol J-F, Gray DG (1996) Effects of Ionic Strength on the Isotropic–Chiral Nematic Phase Transition of Suspensions of Cellulose Crystallites. Langmuir 12:2076–2082. https://doi.org/10.1021/la950133b
8. Dong Z, Ye Z, Zhang Z, et al (2020) Chiral Nematic Liquid Crystal Behavior of Core-Shell Hybrid Rods Consisting of Chiral Cellulose Nanocrystals Dressed with Non-chiral Conformal Polymeric Skins. Biomacromolecules 21:2376–2390. https://doi.org/10.1021/acs.biomac.0c00320

9. Elazzouzi-Hafraoui S, Putaux JL, Heux L (2009) Self-assembling and chiral nematic properties of organophilic cellulose nanocrystals. J Phys Chem B 113:11069–11075. https://doi.org/10.1021/jp900122t
10. Haouache S, Jimenez-Saelices C, Cousin F, et al (2022) Cellulose nanocrystals from native and mercerized cotton. Cellulose 29:1567–1581. https://doi.org/10.1007/s10570-021-04313-8
11. Harris AB, Kamien RD, Lubensky TC (1999) Molecular chirality and chiral parameters. Rev Mod Phys 71:1745–1757. https://doi.org/10.1103/revmodphys.71.1745
12. Heux L, Chauve G, Bonini C (2000) Nonflocculating and chiral-nematic self-ordering of cellulose microcrystals suspensions in nonpolar solvents. Langmuir 16:8210–8212. https://doi.org/10.1021/la9913957
13. Honorato-Rios C, Lehr C, Schütz C, et al (2018) Fractionation of cellulose nanocrystals: enhancing liquid crystal ordering without promoting gelation. NPG Asia Mater 10:455–465. https://doi.org/10.1038/s41427-018-0046-1
14. Jiang W, Qu ZB, Kumar P, et al (2020) Emergence of complexity in hierarchically organized chiral particles. Science (80-) 368:642–648. https://doi.org/10.1126/science.aaz7949
15. Lopez M, Bizot H, Chambat G, et al (2010) Enthalpic studies of xyloglucan-cellulose interactions. Biomacromolecules 11:1417–1428. https://doi.org/10.1021/bm1002762
16. Mitov M (2017) Cholesteric liquid crystals in living matter. Soft Matter 13:4176–4209. https://doi.org/10.1039/c7sm00384f
17. Orts WJ, Godbout L, Marchessault RH, Revol JF (1998) Enhanced ordering of liquid crystalline suspensions of cellulose microfibrils: A small angle neutron scattering study. Macromolecules 31:5717–5725. https://doi.org/10.1021/ma9711452
18. Parton TG, Parker RM, van de Kerkhof GT, et al (2022) Chiral self-assembly of cellulose nanocrystals is driven by crystallite bundles. Nat Commun 13:1–9. https://doi.org/10.1038/s41467-022-30226-6
19. Revol JF, Bradford H, Giasson J, et al (1992) Helicoidal self-ordering of cellulose microfibrils in aqueous suspension. Int J Biol Macromol 14:170–172. https://doi.org/10.1016/S0141-8130(05)80008-X
20. Schütz C, Agthe M, Fall AB, et al (2015) Rod Packing in Chiral Nematic Cellulose Nanocrystal Dispersions Studied by Small-Angle X-ray Scattering and Laser Diffraction. Langmuir 31:6507–6513. https://doi.org/10.1021/acs.langmuir.5b00924
21. Schütz C, Bruckner JR, Honorato-Rios C, et al (2020) From equilibrium liquid crystal formation and kinetic arrest to photonic bandgap films using suspensions of cellulose nanocrystals. Crystals 10
22. Sun Q, Lutz-Bueno V, Zhou J, et al (2022) Polymer induced liquid crystal phase behavior of cellulose nanocrystal dispersions. Nanoscale Adv 4:4863–4870. https://doi.org/10.1039/d2na00303a
23. Voisin H, Vasse A, Bonnin E, Capron I (2023) Influence of Low-Molar-Mass Xyloglucans on the Rheological Behavior of Concentrated Cellulose Nanocrystal Suspensions. Biomacromolecules 24:358–366. https://doi.org/10.1021/acs.biomac.2c01172

24. Yi J, Xu Q, Zhang X, Zhang H (2008) Chiral-nematic self-ordering of rodlike cellulose nanocrystals grafted with poly(styrene) in both thermotropic and lyotropic states. Polymer (Guildf) 49:4406–4412. https://doi.org/10.1016/j.polymer.2008.08.008

Figures

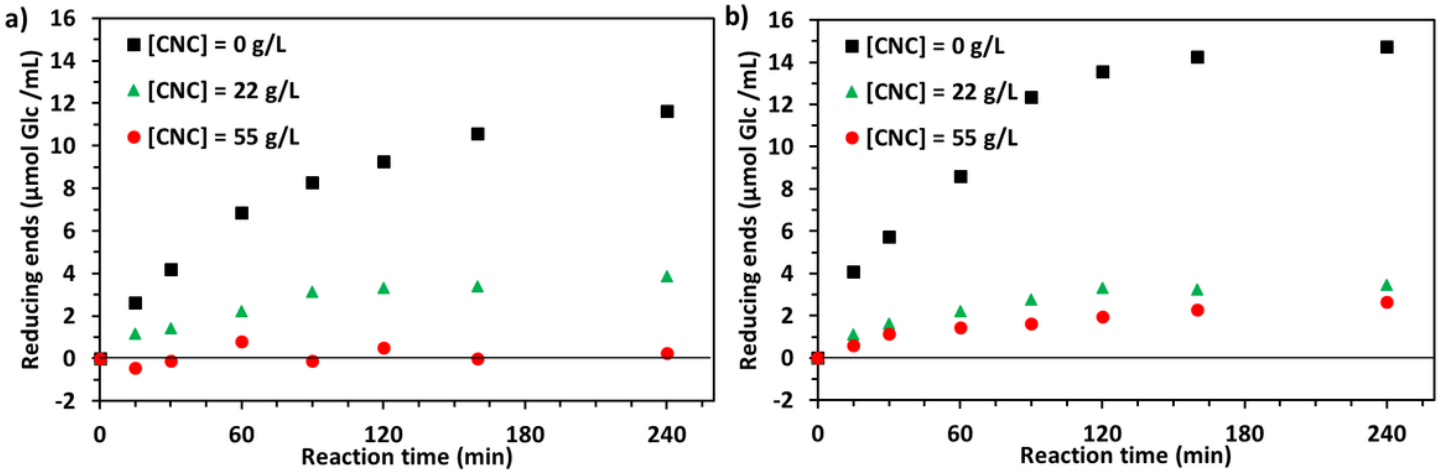

Figure 1

Appearance of glucose reducing ends generated by enzymatic degradation of xyloglucans with different Mw (20,000 g/L (a), 40,000 g/L(b)) mixed with increasing concentrations of CNC between 0 g/L and 55 g/L

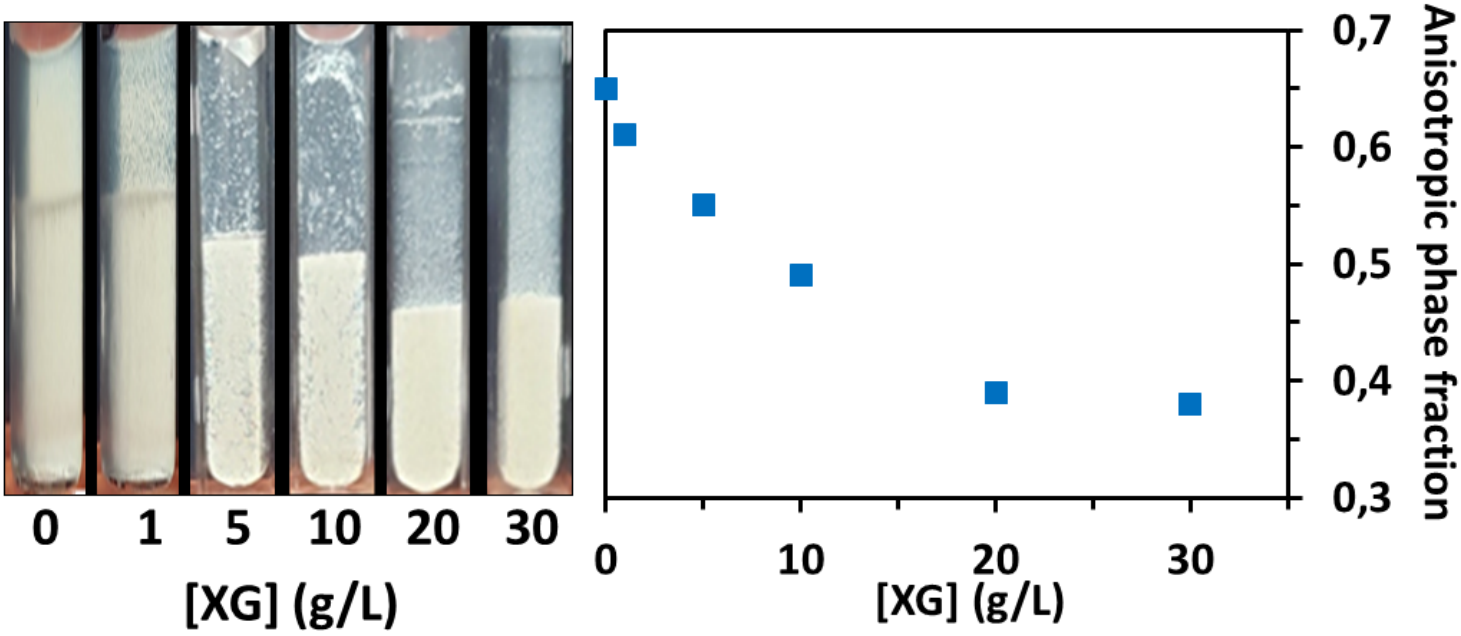

Figure 2

Pictures of tubes between crossed polarizers containing 60 g/L CNC suspension mixed with various XG concentration after 5 days and evolution of anisotropic phase volume fraction as a function of XG concentration

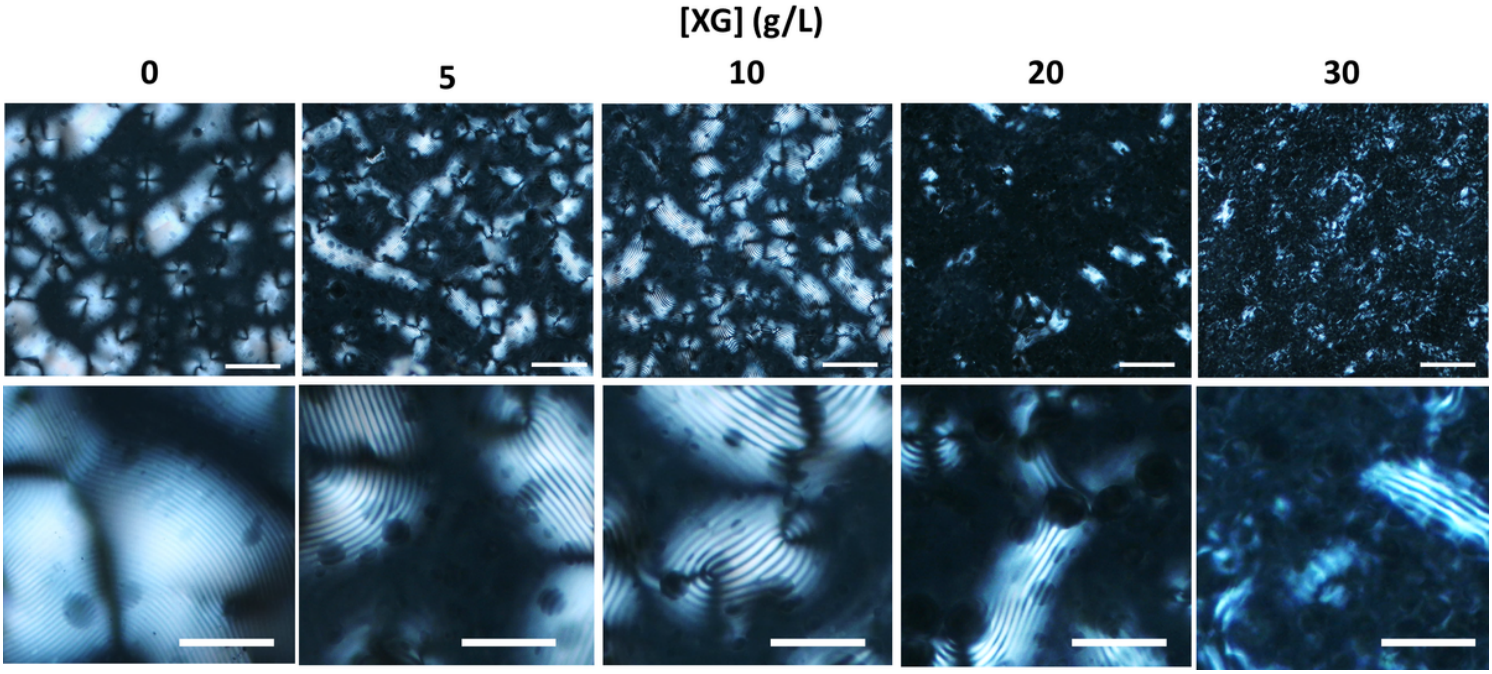

Figure 3

Evolution of the pitch in the full suspensions, just after mixing CNC at 60 g/L with various XG concentrations measured by image analysis; scale bars on the upper rows are 200 µm, scale bars on the lower rows are 80 µm

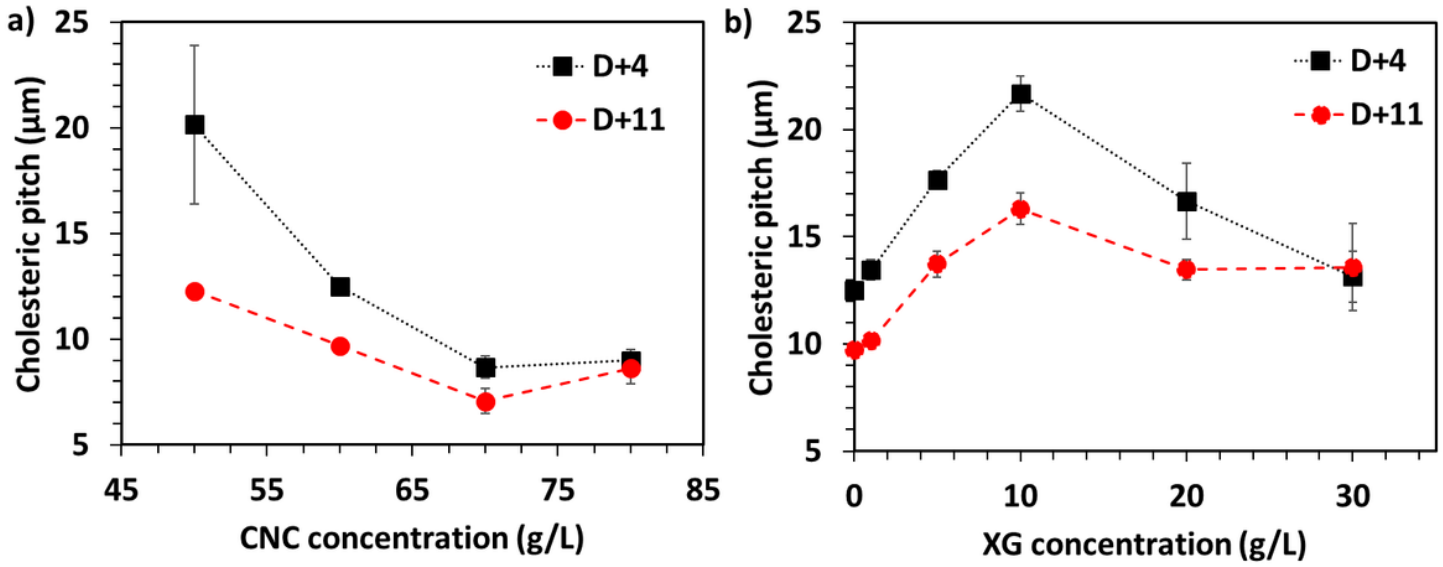

Figure 4

Evolution of the cholesteric pitch of pure CNC suspension at various CNC concentrations (a) and of a 60 g/L CNC suspension mixed with various amounts of XG (b), 4 and 11 days after preparation

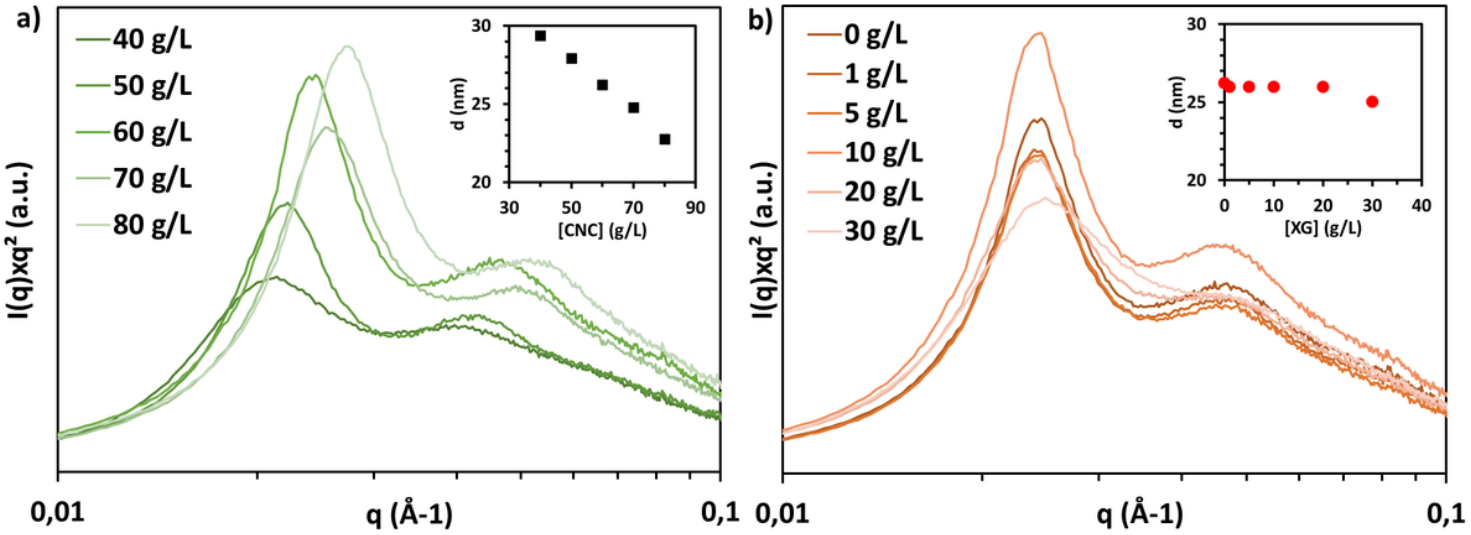

Figure 5

Small-angle X-ray scattering (SAXS) in Kratky representation ($I \times q^2$) against the scattering vector of (a) pure CNC suspensions at various concentrations from 40 to 80 g/L; and (b) a 60 g/L CNC suspension mixed with various XG concentrations from 0 to 30 g/L. The insets represent the evolution of the interparticular distance *d* calculated from the position of the peak

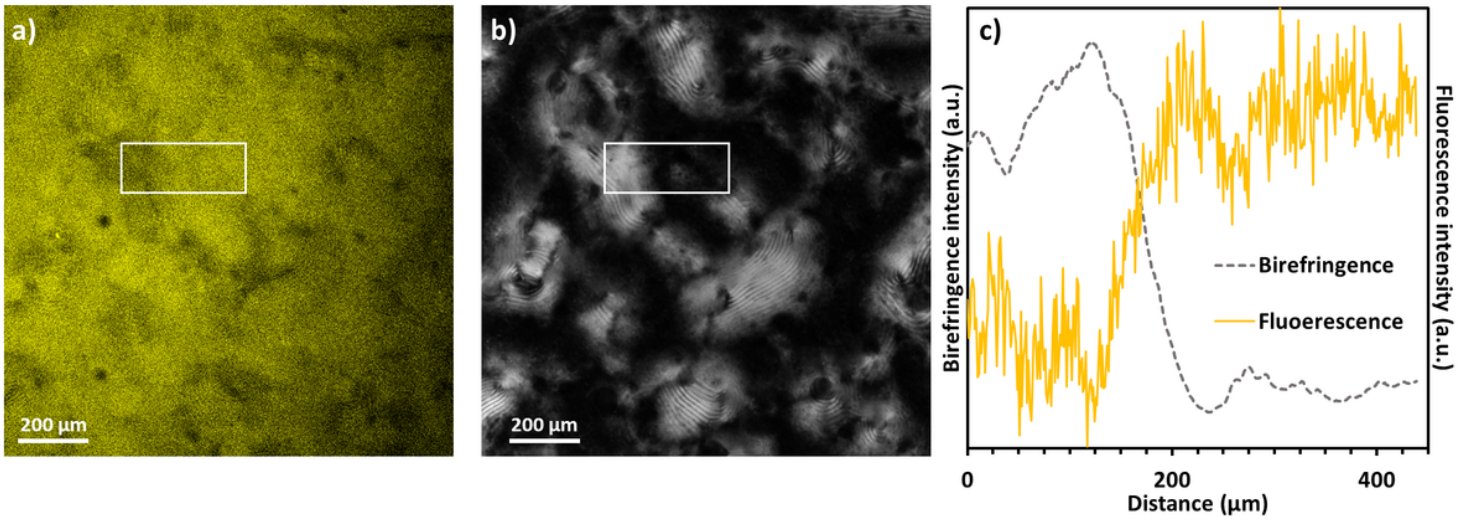

Figure 6

(a) Confocal fluorescence microscopy and POM (b) of a 60 g/L CNC suspension with 10 g/L of XG fluorescently labeled with FITC; (c) intensity profiles of the birefringence and fluorescence intensities from the white rectangle on (a) and (b), vertically integrated and from left to right

Supplementary Files

This is a list of supplementary files associated with this preprint. Click to download.

- SIcholestericVf.docx